ACS OMEGA

Article

Cite This: ACS Omega 2018, 3, 17751−17761

http://pubs.acs.org/journal/acsodf

Ionic Liquid-Based Catanionic Coacervates: Novel Microreactors for Membrane-Free Sequestration of Dyes and Curcumin

Ankit Shah,[†] Muzammil Kuddushi,[†] Sargam Rajput,[†] Omar A. El Seoud,[‡] and Naved I. Malek*[,†]

[†]Applied Chemistry Department, S.V. National Institute of Technology, Surat 395007, Gujarat, India

[‡]Institute of Chemistry, The University of Sao Paulo, 748 Prof. Lineu Prestes Av., Sao Paulo SP 05508-000, Brazil

Supporting Information

ABSTRACT: Surfactant-mediated coacervates are termed as the new age microreactors for their ability to spontaneously sequester the molecules with varied polarities and functionalities. Efforts to emulate this applicability of coacervates through synthetic control of surfactant structures are finding success; however, there is little understanding of how to translate these changes into tailor-made properties. Herein, we designed 3-methyl-1-(octyloxycarbonylmethyl)imidazolium bromide (C_8EMeImBr), an ester-functionalized ionic liquid-based surfactant, which shows better surface active properties than the nonfunctionalized and conventional cationic surfactant and forms complex coacervates over the broad range of concentration with sodium salicylate (NaSal). Mono- and divalent cations as well as ionic strength, viscosity, and time-dependent stability of the coacervates had also been addressed in order to study whether these coacervates could work as microreactors to encapsulate various molecules. The anionic charged complex coacervates with sponge morphology and honey comb-like interior show good efficiency to sequester cationic dyes from water because of electrostatic and hydrophobic interactions and good encapsulation efficiency for curcumin owing to their high surface area. Results suggest that ionic liquid-based coacervates studied here could be exploited as a novel low-cost, effective, and environmentally benign alternative to sequester dyes from the contaminated water and their recovery.

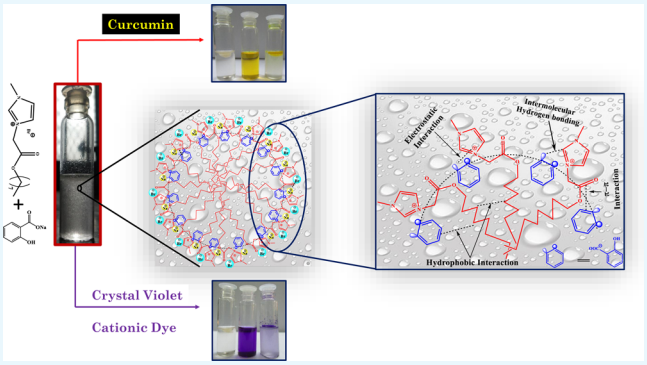

1. INTRODUCTION

Synergistic interactions between the oppositely charged surfactants or ionic surfactants with inorganic and organic electrolytes lead to the formation of various morphological architectures, both in their pure state and in the presence of various external additives.[1,2] The shape and size of these morphological architectures depend on the (i) structural architecture of the individual components of the mixture, (ii) composition of the mixture, and (iii) various solution conditions including pH, temperature, and ionic strength of the solution.[1,2] Judiciously selecting any of these conditions separately or in a group could be advantageous in designing aggregates with varied shapes and sizes including various cell mimetic structures such as vesicles, hydrogels, and coacervates.[1,2] Among these, coacervates, the new age microreactors, are formed as a result of the subtle balance between a range of interactions in the solutions, that is, the electrostatic, hydrophobic, hydrogen bonding, van der Waals forces, and other weak interactions.[3] The ability to preconcentrate various solubizates including dyes, drugs, metal ions, and biomolecules with adjustable sequestering ability makes coacervates low-cost membrane-free microreactors or cell mimetic systems (for biomolecules).[4,5]

Various traditional surfactant systems including nonionic and ionic surfactants form coacervates in their pure form (simple coacervates) as well as in the presence of various external additives (complex coacervates).[6−11] Among these, nonionic surfactant-based coacervates were used to sequester the organic compounds through hydrogen bonding and hydrophobic interactions.[6,7] The efficiency of these coacervates could be enhanced through increasing the hydrophobic character of the nonionic surfactant. It was reported that the preconcentration factor of the nonionic/ionic surfactant mixture is higher than that of the neat nonionic surfactant.[8] This could improve the sequestration ability of the coacervates for the charged organic solutes. Compared to the nonionic surfactant-based coacervates, ionic surfactant-based coacervates provide more binding sites to the analysts as the formation of coacervates are controlled by electrostatic and cation−π interactions apart from the hydrophobic and hydrogen bonding and van der Waals interactions.[9] These interactions, and as a result coacervation, could be tailor-made using hydrotopes in the surfactant-based coacervation system.[10] The catanionic mixture thus formed exhibits superior sequestration ability because of their better surface activity, lower critical micelle concentration (cmc), and then the

Received: September 20, 2018
Accepted: December 4, 2018
Published: December 19, 2018

DOI: 10.1021/acsomega.8b02455
ACS Omega 2018, 3, 17751−17761

individual components of the mixture. Various analysts could be sequestered within these complex coacervate systems including dyes, drugs, and biomolecules. Sequestration of dyes within the coacervate systems is based on the charge on the coacervates.[11−13] Reversible compartmentalization of biomolecules had been achieved through the complex coacervation composed of RNAs with cationic peptides.[14] Chiappisi et al. demonstrated the sequestration of Sudan red dye within the coacervates formed through the interaction of oppositely charged chitosan and alkylethoxy carboxylate.[11,12] Orange OT was sequestered by the coacervates formed through interacting poly(diallyldimethylammonium chloride) with the SDS/Triton-X 100 mixture.[13] Looking at above-mentioned characteristics of ionic surfactant-based coacervates, it is manifested that one can enhance the sequestration ability of the ionic surfactant coacervates by changing their structure.

Recently, ionic liquids (ILs) are studied for their superior interfacial and micellar properties than the conventional surfactants and are also termed as surface-active ILs or IL-based surfactants (ILBSs).[15−17] Ning et al. studied the IL-based coacervates as an adsorbent for the extraction of malachite green, crystal violet (CV), and methylene blue dyes.[18] We are engaged in studying interfacial and micellar properties of the traditional surfactants as well as ILBSs with nonfunctionality in their neat form and through various external additives.[19,20] Studies pertaining to ILBSs with additional functionality are as yet limited, and it is part of our recent and future research endeavor. Introducing functionality makes these novel amphiphiles more task-specific. For example, replacing the methyl group with $-CH_2COOH$ or introducing the vinyl functionality within the head group of the ILBSs improves the surface activity of the latter.[21,22] The impact of the functionality is not limited to only surface activity. The "green credentials" of the ILBSs can also be improved. For example, the toxicity of the ILs can be reduced by incorporating the ether functionality in the side chain of the imidazolium-based ILs.[23] Ester functionality significantly improved the surface and biological activity as well as the biodegradability of the imidazolium- and pyridinium-based ILs.[24]

In a quest to design cost-effective, more efficient, and environmentally benign system to sequester various functional molecules, herein, we design the complex coacervate-based microreactors through the catanionic approach. The catanionic complex coacervates were designed through interacting ILBS, 3-methyl-1-(octyloxycarbonylmethyl) imidazolium bromide (C_8EMeImBr), and sodium salicylate, NaSal, over a broad range of composition. The structure of C_8EMeImBr and NaSal is given in Scheme 1. The stability of the complex coacervates had also been studied in the presence of mono- and divalent cations as well as various solution conditions such as time, ionic strength, and viscosity. These membrane-free microreactors with anionic charge spontaneously sequester cationic dyes owing to the electrostatic and hydrophobic interactions and encapsulate curcumin because of the larger surface area.

Scheme 1. Molecular Structures of (a) 3-Methyl-1-(octyloxycarbonylmethyl) Imidazoliumbromide (C_8EMeImBr) and (b) Sodium Salicylate (NaSal)

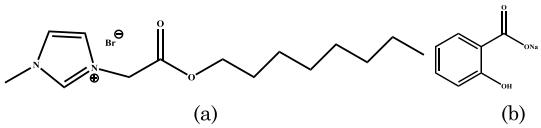

(a) (b)

2. RESULTS AND DISCUSSION

A subtle balance of interactions such as electrostatic, hydrophobic, hydrogen bonding, cation−π, and $\pi-\pi$ interactions between the oppositely charged substrate (anionic Sal) and micellar aggregate of C_8EMeImBr leads to the formation of a complex coacervates phase and dilute aqueous phase of C_8EMeImBr.[3] The complex coacervate phase was obtained at the range of mixture composition, that is, at a fixed concentration of C_8EMeImBr (112.5 mM) and at a range of NaSal concentration (100−400 mM). The phase behavior of the mixture was studied through combining the turbidity data and visual observation data. We used physical, spectroscopic, and microscopic methods to detect the morphological changes in the mixture as a function of increasing concentration of NaSal. cmc of C_8EMeImBr measured through surface tension is 45 mM, which was then compared with the traditional surfactant and nonfunctionalized ILBS with analogous alkyl chain length. All measurements were performed on the micellar solutions of C_8EMeImBr. The complex coacervates were used to sequester dyes [Methyl Orange (MO), Allura Red (AR), CV, and rhodamine B (RB)] and to encapsulate curcumin.

2.1. Adsorption of C_8EMeImBr at the Solution/Air Interface. Figure 1 depicts the surface tension plot of the

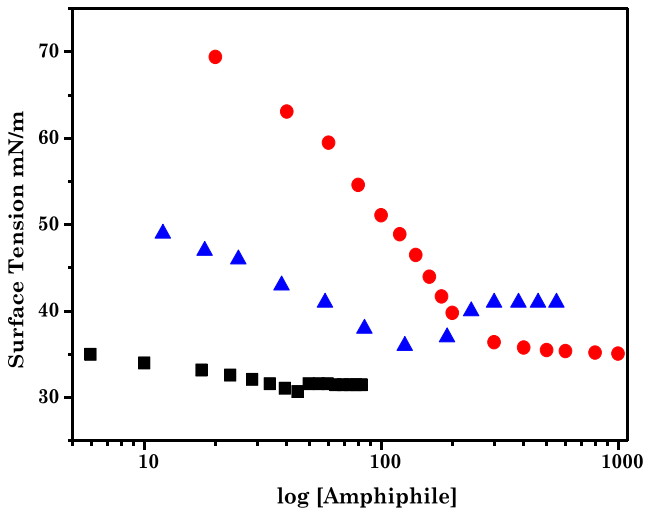

Figure 1. Surface tension versus logarithm of the concentration curve of C_8EMeImBr (■), C_8MeImBr (blue triangle), and C_8TABr (red circle) curves at 25 °C in aqueous medium.

C_8EMeImBr solution along with the nonfunctionalized ILBS, 3-methyl-1-octylimidazolium bromide (C_8MeImBr), and conventional surfactant, and octyltrimethyl ammonium bromide (C_8TABr), with an identical alkyl chain length (n = 8) in aqueous medium as a function of logarithmic concentration of amphiphiles at 25 °C. As reported, with the increasing concentration of C_8EMeImBr, the adsorption of C_8EMeImBr on the air/water interface increases which decreases the surface tension. At a certain concentration, surface tension attains a minimum value before micellization. Traditional ionic and nonionic surfactants as well as functionalized and non-functionalized ILBS with surface active impurities show similar surface tension behavior.[24,25] We performed several purifica-

DOI: 10.1021/acsomega.8b02455
ACS Omega 2018, 3, 17751−17761

Table 1. Calculated Parameters from Surface Tension Data for C_8EMeImBr, C_8MeImBr and, C_8TABr at 25 °C[a]

1ILBS	cmc (mM)	γ_{cmc} (mN/m)	π_{cmc} (mN/m)	$\Gamma_{max} \times 10^6$ (mol/m^2)	A_{min} (Å^2)	Refs
C_8EMeImBr	43	31.0	41.0	2.58	64	24
C_8EMeImBr	45	30.7	41.3	2.44	68	this work
C_8MeImBr	170	41.3	30.7	1.34	124	33
C_8TABr	261	39.8	32.2	1.91	52	34

[a]The uncertainties in the calculated parameters are as follows: $\gamma_{cmc} = \pm 0.1$ mN/m; $\pi_{cmc} = \pm 0.1$ mN/m; $\Gamma_{max} = \pm 0.2 \times 10^{-6}$ mol/m^2; $A_{min} = 0.5$ Å^2.

tion steps to remove this, but no significant change in the surface tension results was observed. Formation of micelles and the surface monolayer before micellization might be the cause for this surface tension minimum.[25] Herein, we assigned the concentration associated with this surface tension minimum as the cmc of C_8EMeImBr, which is in good agreement with the reported literature.[24] cmc values for C_8EMeImBr, nonfunctionalized (C_8MeImBr), and conventional cationic surfactants (C_8TABr) are in order: C_8EMeImBr (45 mM) < C_8MeImBr (170 mM) < C_8TABr (261 mM).[24−27] The lower cmc of the ester-functionalized ILBS is due to the (i) hydration of the ester group within the head group, which decreases the repulsion of the head groups at the air−water interface and (ii) the intramolecular hydrogen bonding within the head groups, which is favored by the close proximity of the ester group to the imidazolium ring.

The comparison of data pertaining to surface tension at cmc (γ_{cmc}), the effectiveness of surface tension reduction (π_{cmc}), the maximum surface excess concentration (Γ_{max}), the minimum area occupied per amphiphilic molecule (A_{min}) at the solution/air interface for C_8EMeImBr, C_8MeImBr, and C_8TABr in aqueous medium are reported in Table 1. γ_{cmc} for C_8EMeImBr is lower than that of C_8MeImBr and C_8TABr, that is, introducing the functionality increases the efficiency of the ILs to reduce the surface tension of water. The surface pressure at the cmc (π_{cmc}) for the studied ester-functionalized ILBS, C_8EMeImBr, is higher than that of the conventional and nonfunctionalized ILBS, that is, C_8TABr and C_8MeImBr, respectively. The higher values of Γ_{max} for the ester-functionalized ILBSs than the C_8MeImBr and C_8TABr indicate that ester-functionalized ILBSs accumulate in greater amount at the air/water interface than others. A_{min} calculated for C_8EMeImBr is lower than the nonfunctionalized and −COOH-functionalized ILBS as well as for C_8TABr.[28−30] This concludes that C_8EMeImBr forms more compact structures on the surface than the nonfunctionalized and −COOH-functionalized ILBS as well as the traditional surfactant.

The geometry and size of the aggregates influence the applications of the amphiphiles. We employed the well-known Israelachvilis ratio to predict the shape of the aggregates for C_8EMeImBr.[31] Combining the experimentally determined values of A_{min} and using the Tanford formula,[32] we calculated the packing parameter (P); which was less than 0.33, indicating that the aggregates for C_8EMeImBr are spherical in shape near its cmc.[24] The size and shape of the aggregates could be modulated through interaction of the amphiphiles with various external additives. Among these, hydrotropes are well known as they are structurally similar to surfactants except the alkyl chain. They interact electrostatically as well as hydrophobically with the ionic surfactants, leading to the change in the shape and size of the micellar aggregates. Among the range of hydrotopes, sodium salicylate, because of its well-established surface activity and self-aggregation behavior, is tested in the present study to change the shape and size of the micellar aggregates of the aqueous solution of C_8EMeImBr.

In our earlier publication, we had reported the transition of spherical micellar aggregates of the nonfunctionalized ILBSs into the vesicles through addition of the external additives including NaSal.[35,36] For NaSal as the additive, several authors have reported the formation of rodlike micelles, wormlike micelles, vesicles, and hydrogels near the equimolar concentration for the traditional cationic surfactants and for ILBSs. We represented these comparison data in Table SI-1 in the Supporting Information. For the first time, in the present investigation, we observed the formation of complex coacervates near the charge neutralization concentration, that is, at equimolar concentration. The coacervate droplets formed are separated from the aqueous solution of C_8EMeImBr and are observed at the upper side of the sample tube. The phase behavior of the aqueous C_8EMeImBr solution in the presence of various concentrations of NaSal is explained herewith in detail through visual observation and turbidity measurement.

As reported in Figure 2, turbidity of the mixture increases upto a certain concentration, stays practically constant, and

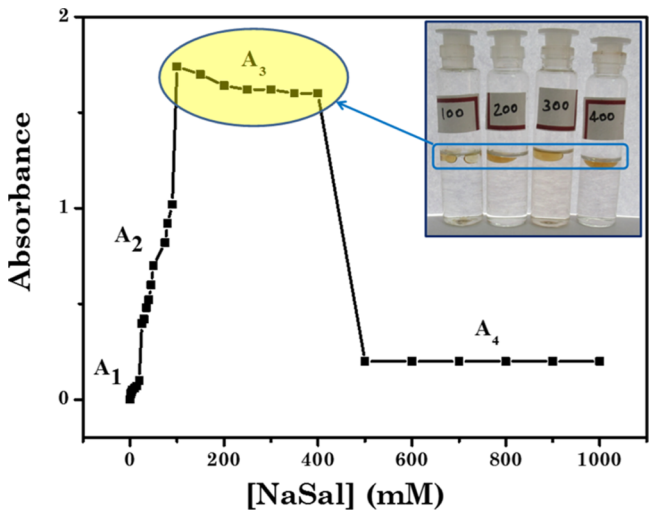

Figure 2. Turbidity curve showcasing the phase boundaries of the C_8EMeImBr/NaSal system with 112.5 mM concentration of C_8EMeImBr and variable concentrations of NaSal.

then decreases. To understand the effect of NaSal concentration on the shape and size of the micellar aggregates of C_8EMeImBr, we divided the turbidity behavior in four portions, A_1, A_2, A_3, and A_4 based on the concentration of NaSal. With the increasing concentration of NaSal, pH of the neat micellar solutions of C_8EMeImBr changes from 2.61 to 7.41 for the addition of 1000 mM of NaSal. The pK_a of NaSal in water is 2.79, that is, NaSal is present as (Sal^-) under our experimental conditions (pH of solution with 2 mM NaSal was 2.84). We can safely assume that the micellar changes occurred

DOI: 10.1021/acsomega.8b02455
ACS Omega 2018, 3, 17751−17761

in the solution are due to the electrostatic interactions between the cationic micelle and the anionic Sal^-, as indicated for the drug-induced micellar transition in the ILBS solution and other catanionic systems.[10,35,36] Region A_1 belongs to the concentration (C_{NaSal} < 10 mM) where transparent solution with nearly zero turbidity was observed (Figure 2). This indicates the weaker interaction between NaSal and C_8EMeImBr that forms only smaller-sized aggregates. Beyond A_1, with the increasing concentration of NaSal, turbidity increases may be due to the increased size of the aggregates because of the stronger electrostatic and hydrophobic interaction with the increased number of NaSal in solution. Electrostatic interactions between $[C_8EMeIm]^+$ with the carboxylate anion of the NaSal and hydrophobic interactions between the alkyl chain of C_8EMeImBr and the aromatic group of NaSal increased the packing and eventually the size of the aggregates. With further increase in C_{NaSal}, in the A_3 region, the turbidity sharply increases to a very large value (the data in the A_3 region of Figure 2 are obtained through diluting the coacervate phase 10 times with water) and formation of droplets occurs that are phase-separated from the aqueous C_8EMeImBr solution with time. This may be due to the association of the C_8EMeImBr/NaSal aggregates, which leads to the formation of liquid−liquid phase separation. The complex coacervate droplets were observed between 100 and 400 mM concentrations of NaSal. Beyond the A_3 region, turbidity decreases with the formation of clear solution. This may be due to the formation of catanionic complexes which is due to the dissolution of coacervates into excess NaSal. The coacervation region was observed around the charge neutralization point between cationic C_8EMeImBr and anionic NaSal, as evidenced through the zeta potential results (Table 2). Zeta potential

Table 2. Zeta Potential of the Selected Complex Coacervates at Different Concentrations of NaSal

[NaSal]/(mM)	Zeta potential/(mV)
100	9.86
200	−7.26
300	−8.77
400	−8.91

results indicate that the charge on the coacervate droplets depends on the concentration of NaSal. Our results are in accordance to the results reported by Douliez et al., where the authors have reported the catanionic droplets with positive and negative charge based on the ratio of cetylpyridinium chloride to decanoic acid for different amounts of NaOH.[37] Further, as reported in Table SI-2, for conventional and ILBS systems, only the aggregates that are rodlike and wormlike with vesicles and hydrogels are reported.[10] Reports pertaining to the formation of complex coacervates in the ILBS system are not yet reported as per our knowledge.

Colloidal solution in region A_3 separates into two equilibrium phases with time: a viscous coacervate phase rich in the colloidal material and a low viscous aqueous phase with lower concentration of the colloidal material. The down coacervate phase is colorless and isotropic and has higher viscosity, which is consistent with the matrix of elongated micelles.[38] Thus, the one with up to 95% water and the other with 99−100% water do not freely mix with each other.[38] We perform dynamic light scattering (DLS), optical microscopy, and field emission scanning electron microscopy (FESEM) measurements to deduce the size and morphology of the complex coacervate droplets. The polydisperse suspension of the spherical droplets is of the size 100−500 μm as measured through DLS while mixing C_8EMeImBr (112.5 mM) and NaSal (100−400 mM) in water and is evidenced through optical microscopy (Figure 3). With the increasing concentration of NaSal, the size decreases. At 200 mM concentration of NaSal, yolk−shell type particles may be composed of shells (hollow spherical particles) with a smaller yolk (solid sphere) in their interior (Figure 3b). The complex coacervates prepared through mixing 112.5 mM of C_8EMeImBr and 200 mM of NaSal were further visualized using epifluorescence images (Figure 4a), where the coacervate droplets were labeled using rhodamine 6G. The concentration of the dye was taken very low in order to minimize the dye−coacervate interaction. The morphology of these "yolk−shell" particles visible in Figures 3b and 4a was further analyzed using FESEM and found that these complex coacervate phases have "sponge" morphology (Figure 4b). The three-dimensional structure of the coacervate droplet is visible at 4950 instrument magnification with the honey comb-like interior, with 2.67−7.22 μm pores. Menger et al. reported a similar sponge morphology for simple coacervates prepared from the aqueous zwitterionic gemini surfactants.[39] The morphology as well as the interior structure could be applicable in various technological applications including encapsulating various substrates.

The subtle balance of interactions responsible for the formation of complex coacervates within the catanionic system composed of $NaSal^-/C_8$EMeImBr is characterized through measuring the Fourier transform infrared (FT-IR) spectrum of the partially dried coacervate samples and was compared with neat C_8EMeImBr. Figure 5 shows the changes in the methylene peaks in the infrared absorption peaks for neat C_8EMeImBr and coacervate samples. As observed in Figure 5, the asymmetric and symmetric stretching vibrations of $-CH_2$ groups are shifted to higher wave numbers, that is, from 2922 and 2854 cm^{-1} to 2928 and 2859, respectively, as compared to the neat C_8EMeImBr. The change in this region corresponds to the gauche/trans conformations. The shift of frequency toward a lower value corresponds to the ordered trans conformation, whereas the shift of frequency toward a higher value corresponds to the disordered gauche conformation. In the present investigation, the shift of frequency toward higher wavenumber suggests that the methylene chain observes gauche conformation in the coacervate phase because of the increased hydrophobic interactions between the alkyl chain of C_8EMeImBr and the aromatic group of NaSal.

The C−N stretching vibration (asymmetric and symmetric) in the cationic ring, which is located at 1470 and 1462 cm^{-1} in powder C_8EMeImBr is shifted to 1479 and 1456 cm^{-1} for the coacervates. Further, −C−O stretching vibration located at 1180 cm^{-1} in the pure C_8EMeImBr is shifted to 1168 cm^{-1}. This indicates the strong electrostatic interaction between Sal^- and C_8EMeIm^+.[40] Further, the ester group absorption peak which is at 1747 cm^{-1} for the pure C_8EMeImBr is shifted to 1741 cm^{-1} for the coacervates, that is, the ester group is likely to be more hydrated in the coacervates that are formed at higher concentrations of NaSal.[40]

2.2. Stability Study of Complex Coacervates. In order to serve the complex coacervates formed here as the microreactors, we analyzed the stability of the studied complex coacervates in various solution conditions, such as spontaneity

DOI: 10.1021/acsomega.8b02455
ACS Omega 2018, 3, 17751−17761

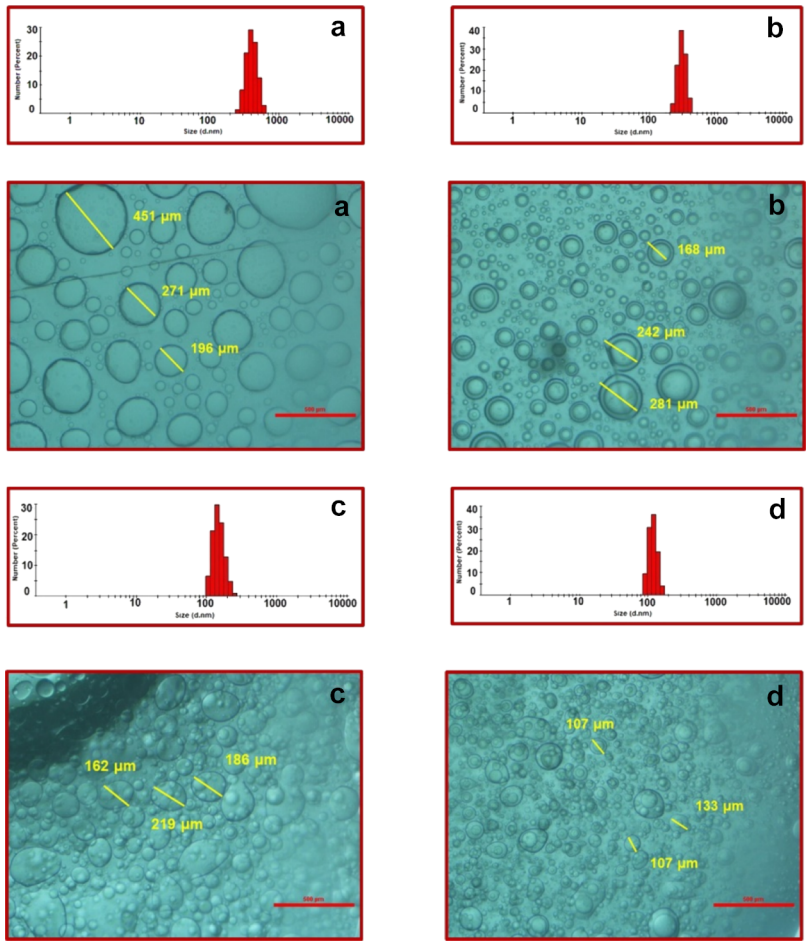

Figure 3. DLS and optical microscopy images of the complex coacervates with C_8EMeImBr (112.5 mM) and (a) 100, (b) 200, (c) 300, and (d) 400 mM concentrations of NaSal (scale bar = 500 μm).

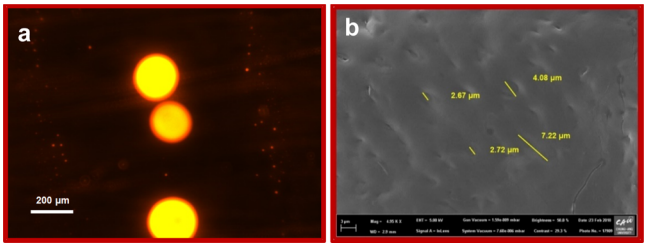

Figure 4. (a) Epifluorescence image of complex coacervates prepared through mixing 112.5 mM of C_8EMeImBr and 200 mM of NaSal and rhodamine 6G (2.04×10^{-3} mM). Scale bars: 200 μm. (b) FESEM image of the complex coacervate phase with C_8EMeImBr (112.5 mM) and NaSal (200 mM) in water.

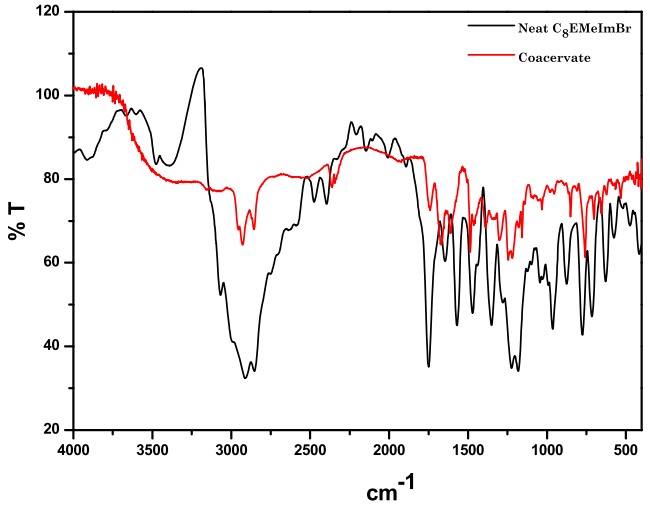

Figure 5. FTIR Spectrum of neat C_8EMeImBr and complex coacervates formed through 112.05 mm of C_8EMeImBr and 200 mM of NaSal.

of formation, ionic strength, and viscosity of the solution, and in the presence of mono and divalent cations.[41−43] As shown in Figure 3, the droplet size of the complex coacervates varied from 100 to 500 nm through varying the concentration of NaSal from 100 to 400 mM. At 100 mM concentrations of NaSal, coacervates are positively charged (zeta potential data, Table 2, vide supra) and are formed by the subtle balance of electrostatic interactions between Sal^- and C_8EMeIm^+ and hydrophobic interactions between the aromatic part of NaSal and alkyl chain of the C_8EMeImBr. The size of the droplets is bigger at this concentration of NaSal because of the relatively same number of cations and anions in the solution. Therefore, at 100 mM concentration of NaSal, coacervation takes place spontaneously and the size of the coacervate droplets is bigger. However, with increasing the concentration of NaSal beyond 112.5 mM, the excess salt present in the solution dissolves the catanionic complex coacervates and disfavors the coacervation, which decreases the size of coacervate droplets. Thus, ionic strength is an important factor for the coacervate morphology

DOI: 10.1021/acsomega.8b02455
ACS Omega 2018, 3, 17751−17761

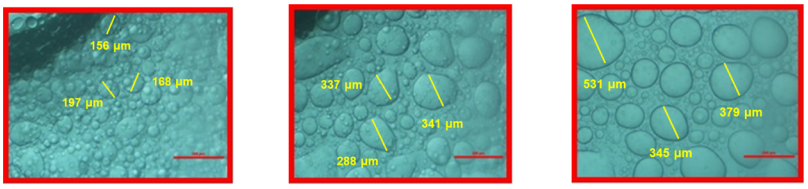

(a) (b) (c)

Figure 6. Optical microscopy images of the complex coacervates with C_8EMeImBr (112.5 mM) and NaSal (300 mM) as a function of time (a) 0, (b) 5, and (c) 10 min. (Scale bar = 500 μm).

as it helps in molecular rearrangement and by that means the coacervation.[42,43]

The coacervate droplets that are formed spontaneously coalesced into a 2.5 mL layer, that is separated from the aqueous layer on resting. Spontaneously formed coacervate droplets are measured under optical microscopy with respect to resting time. Optical micrographs of the coacervate droplets formed through C_8EMeImBr (112.5 mM) and NaSal (300 mM) show that with increasing time from 0 to 15 min, the droplets coagulate with each other and form bigger-sized droplets (Figure 6). After 15 min, no more coagulation takes place, and the size of the droplets remains intact.[37]

The effect of mono- and divalent cations on the stability of the complex coacervates was investigated through the addition of increasing concentration of NaCl, $MgCl_2$, and $CaCl_2$. Solution of NaCl could employ the osmotic pressure across the cell membranes, causing them to burst in their early stage of evolution. We observe that the coacervates were stable in the presence of 400 mM concentration of NaCl. Insensitivity to NaCl by the complex coacervates is likely attributable to the catanionic nature and the stronger counterion binding of Sal^- with C_8EMeIm^+ where associations with external monovalent ions are negligible. The divalent salts, for example, $MgCl_2$ and $CaCl_2$, have the ability to disassemble the fatty acid and amphiphilic compounds, the constituents of the cell membrane, into the crystalline salts. We observe that upto 100 mM concentration of $MgCl_2$, the coacervates are stable, whereas coacervates became destabilized to produce a crystalline salt upon addition of only 100 mM of $CaCl_2$ (Figure SI-1).[37,44]

The droplet size was controlled according to change in internal viscosity of the solution. Higher viscous solution favors smaller-sized droplets, whereas lower viscous solution favors bigger-sized coacervate droplets. We inhibited coalescence of the coacervates to produce stabilized coacervate droplets by increasing the internal viscosity through incorporating 0.15 w/v % solution of sodium alginate (NaAlg). No phase separation was observed after 1 week, and the mean size of the droplets also remained intact (Figure SI-2).[42,44] This indicates that incorporating NaAlg within the C_8EMeImBr/NaSal droplets effectively stabilizes the coacervates.

2.3. Application of the Coacervates in Dye Sequestration and Curcumin Encapsulation. Textile dyes with thermal and light stability are the major pollutants in water resources and are of prime concern. Further, chromophoric and fluorophoric dyes are used to probe the microenvironment of micellar assemblies and to deduce the shape and size of the aggregates.[45,46] Several strategies have been adopted to either remove or preconcentrate these dyes from the aqueous solution.[47] Coacervation-based absorbents have been widely used in medicine, food science, and cosmetics as microreactors.[47,48] Major advantages of coacervation are their ability to perform encapsulation in a purely aqueous medium and the potential for dramatically enriching the desired molecules in the amphiphile-rich coacervate phase.

Herein, we explored the ability of the complex coacervate droplets to sequester the anionic (MO and AR and cationic CV and RB) dyes and curcumin from the aqueous medium. Though sequestration of the dyes by visual inspection is relatively the best option because the coloration of phases after phase separation is direct evidence of this extraction phenomenon, with electron microscopy and UV−visible absorption spectroscopy, we can determine the sequestration of dye quantitatively.

We define the partition coefficient, log P, the molar ratio between the dye dispersed per unit volume in the coacervate phase versus that in the lower dilute phase to further characterize the results of sequestration. log P is expected to give a relative characterization of the sequestration within coacervates droplets. Negative values of log P define that the aqueous phase is richer in the dye concentration, whereas positive values describe the more encapsulation efficiency in the coacervate phase. The values of log P for all of the systems investigated are reported in Table 3. log P has been calculated as per the equation below

$$\log P = \log\left(\frac{C_{\text{coacervate}} - C_{\text{water}}}{C_{\text{water}}}\right)$$

where the numerator and denominator define the concentration of dye in the coacervates and dilute aqueous phase, respectively.

Table 3. Absorption of Various Substrates Using Complex Coacervates

entry	adsorbed substrate	λ, nm	adsorption time, h	log P	adsorbate removal, %
1	MO	463	24	−1.30	4.74
2	AR	504	24	−1.72	1.88
3	CV	580	24	2.00	99.03
4	RB	554	24	2.46	99.65
5	curcumin	430	24	1.34	95.59

The sequestration data obtained for the studied dyes in the complex coacervate droplets formed in the C_8EMeImBr (112.5 mM)/NaSal (200 mM) system are reported in Figures 7 and 8. It is to be mentioned here that at the selected composition, the coacervates are negatively charged (Table 2, zeta potential data, vide supra) and have yolk−shell type particles with sponge morphology as evidenced from Figures 3b and 4b. We believe that the yolk−shell particles with the "sponge" morphology that are composed of a hollow spherical shell and a smaller yolk (solid sphere) in their interior could sequester the dye molecules more efficiently. As reported in

DOI: 10.1021/acsomega.8b02455
ACS Omega 2018, 3, 17751−17761

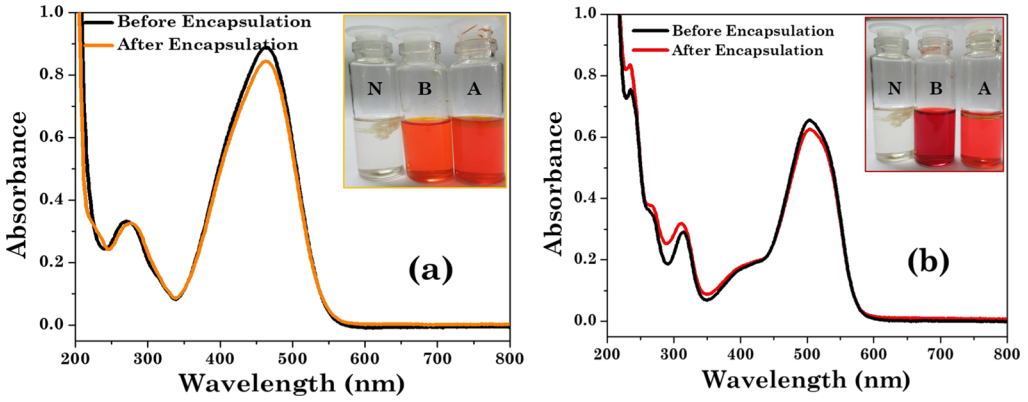

Figure 7. Encapsulation efficiency of the coacervates for MO and AR dyes. UV−vis spectra of the dye (a) before encapsulation (4.05×10^{-5} M) and after encapsulation (3.86×10^{-5}M) for MO and (b) before encapsulation (2.75×10^{-5} M) and after encapsulation (2.70×10^{-5}M) for AR dye. Inset figures demonstrate visual images of neat, before encapsulated, and after encapsulated dyes with N, B, and A, respectively.

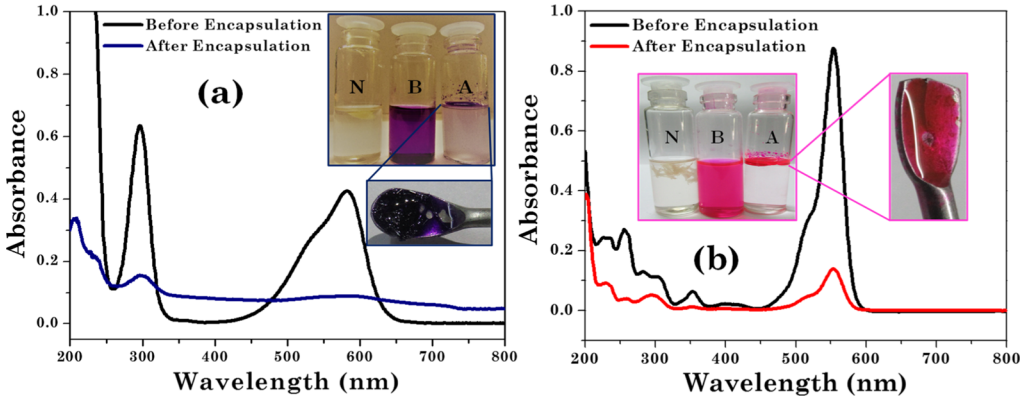

Figure 8. Encapsulation of CV and RB dyes in complex coacervates. UV−vis spectra of the dye (a) before encapsulation (2.45×10^{-3} M) and after encapsulation (2.38×10^{-5} M) for CV and (b) before encapsulation (7.00×10^{-3} M) and after encapsulation (2.43×10^{-5} M) for RB dye. Inset figures demonstrate visual images of neat, before encapsulated, and after encapsulated dyes with N, B, and A, respectively. The encapsulated dye samples extracted in spatula are shown in the inset.

Figure 7, the intensity of the characteristic absorption peak of MO (3.86×10^{-5} M) in the supernatant phase at 463 nm is almost the same as that of MO (4.05×10^{-5} M) in the aqueous phase without coacervates. This means that almost all MO (more than 95%) remains in the aqueous phase, and no MO was extracted by the coacervate phase (Table 3). Optical microscopy images in Figure 10b confirm that the MO dye remains in the aqueous phase rather than the coacervate phase. Similar results are observed for the AR dye (Figures 7 and 10d, Table 3). Contrary to this, polyacrylamide-mediated coacervation of the gemini surfactant absorb 95% MO dye in the coacervate phase (at equimolar concentration).[49] The negatively charged dyes sequestered negligibly, which is evident from their negative values of log *P*. log *P* values for MO and AR are −1.30 and −1.72, respectively (Table 3). As IL-based coacervates are negatively charged (zeta potential results, vide infra), negatively charged dyes are not sequestered within coacervate droplets.

By contrast, all positively charged dyes were sequestered within the upper coacervate phase. Interestingly, CV and RB are fully sequestered in the upper coacervate phase. This was also evidenced from the absorbance and optical microscopy results (Figures 8 and 10a, Table 3). Optical microscopy images in Figure 10a,c confirm that CV and RB remain in the coacervate phase rather than the aqueous phase. The partition coefficient values (log *P*) for CV and RB were found to be 2.92 and 3.33, respectively (Table 3). Positively charged dyes interact with the negatively charged complex coacervates and resulted in higher sequestration.

We adopted a similar method as we applied for the dyes for the encapsulation of curcumin. Despite poor solubility in water, curcumin is used as an antimicrobial, anti-inflammatory, antioxidant, and wound healing agent.[50] The solubility and hence the bioavailability of curcumin has been overcome by several strategies, for example, through encapsulating it within polymer gels and silk fibroin.[50] In the present study, we had successfully loaded 95.59% curcumin within the complex coacervates with the 1.33 log *P* value and is confirmed through absorbance results and optical microscopy images (Figures 9 and 10e, Table 3). The higher efficiency of the complex coacervates to load the curcumin may be due to the higher surface area of the coacervates and the available sites for adsorption due to its internal honey comb-like structure and sponge morphology.

3. CONCLUSIONS

In conclusion, we have proposed IL-based catanionic systems with the ability to self-organize into complex coacervates over a broad range of ionic strength as a step toward novel IL-based membrane-free microreactors. These new age microreactors with "sponge" morphology and a honey comb-like interior can be looked as multicompartmental structures in which analysts

DOI: 10.1021/acsomega.8b02455
ACS Omega 2018, 3, 17751−17761

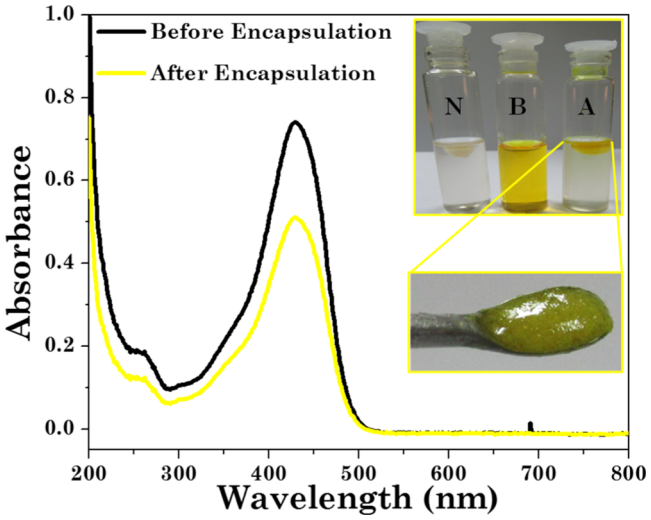

Figure 9. UV−vis spectra of the supernatant phase (diluted by 10 times) of the C_8EMeImBr/NaSal solution mixed with curcumin before (2.70×10^{-3} M) and after (1.19×10^{-4} M) encapsulation. Inset figures demonstrate visual images of coacervate solution, before addition of dye and after encapsulation of the dye.

with varied polarities and functionalities could be sequestered. The complex coacervates are stable with time and upto high concentration of NaCl (400 mM) and $MgCl_2$ (100 mM), whereas they are converted into crystalline salt upon the addition of 100 mM of $CaCl_2$. Moreover, the droplets can be stabilized by reversible hydrogelation by sodium alginate. We have shown that cationic dyes are sequestered within anionic coacervates in high yields by a simple and robust method. These complex coacervates show higher encapsulation efficiency for the curcumin. These findings support a microreactor model that is a more efficient, low-cost, and environmentally benign membrane-free alternative for the removal of dyes from the water as well as the model to preconcentrate them for various applications.

4. MATERIALS AND METHODS

4.1. Materials. All the reagents studied in the present investigation (bromoacetic acid, *n*-octanol, *n*-hexane, ethyl acetate, chloroform, *N*-methyl imidazole, methanol, NaCl, $MgCl_2$, $CaCl_2$, sodium alginate, *p*-toluene sulphonic acid monohydrate, sodium salicylate, CV, MO, AR, RB, and curcumin) were of analytical grade, purchased from Sigma-Aldrich, and used as received.

4.2. Synthesis of ILBS (3-Methyl-1-(octyloxycarbonylmethyl)imidazolium Bromide). Ester-functionalized ILBS 3-methyl-1-(octyloxycarbonylmethyl)-imidazolium bromides, C_8EMeImBr with molecular formula $C_{14}H_{25}BrN_2O_2$ and a molecular weight of 333.26 g/mole, was synthesized in our laboratory following the two-step procedure.[24] Briefly, in the first step, the octyl-2-bromoacetate was synthesized by mixing *n*-octanol (10 mmol, 16 mL) and bromoacetic acid (12 mmol, 8.63 mL) at a volume ratio of 1:1.2. In the mixture, *p*-toluene sulphonic acid monohydrate (1 mmol, 1.92 g) was added as the catalyst, and the reaction mixture was heated at 80 °C on the magnetic stirrer for 4 h. The completion of the reaction was monitored through TLC (*n*-hexane/ethyl acetate, 9:1). The reaction mass was then dissolved in $CHCl_3$ and washed with 100 mL of water (10 mL aliquots). The product was phase separated, and the reaction mass was transferred to a rotary evaporator to remove the solvent and water. Then, the crude product was washed with warm aqueous methanol (methanol/water, 98:2), phase separated and again taken in a rotary evaporator to remove excess methanol and water. Purity of the compound was tested by ^{1}H NMR. In the second step, octyl-2-bromoacetate (10 mmol, 2.51 g) was reacted with *N*-methyl imidazole (10 mmol, 0.80 g) at 90 °C for 2−3 h. TLC with a mobile phase *n*-hexane/ethyl acetate ratio of 9:1 was used to monitor the reaction progress. After cooling the reaction mass to room temperature, the crude product was repeatedly washed with 100 mL diethyl ether (10 aliquots) and then precipitated in cold acetone to yield the functionalized IL with yield of 80%.

4.2.1. Octyl-2-bromoacetate. Yield 92%.^{1}H NMR [Bruker AVANCE 300 spectrometer (400 MHz). $CDCl_3$ as solvent. δ ppm]: δ 0.88 (t, 3H), 1.21−1.30 (m, 10H), 1.64 (m, 2H), 3.87 (s, 2H), 4.20 (t, 2H).

4.2.2. C_8EMeImBr. A white waxy solid with a melting point of 64 °C and yield of 80%. ^{1}H NMR [Bruker AVANCE 300 spectrometer (400 MHz). $CDCl_3$ as solvent. δ ppm]: δ 9.5 (s, 1H), 7.68 (s, 2H), 5.39 (s, 2H), 4.20 (t, 2H), 4.0 (s, 3H), 1.66 (m, 2H), 1.21−1.30 (m, 10H), 0.88 (t, 3H).

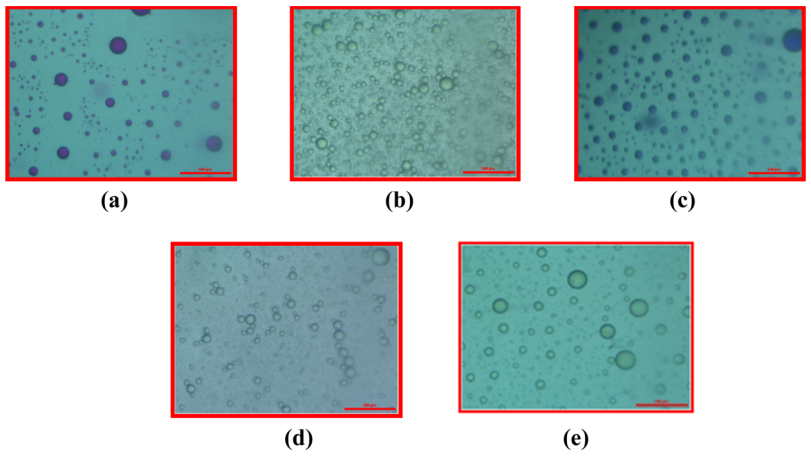

Figure 10. Microscopy image of the coacervate formed by 112.5 mM of C_8EMeImBr and 200 mM of NaSal in the presence of (a) (2.45×10^{-3} M) CV, (b) (4.05×10^{-5} M) MO, (c) (7.00×10^{-3} M) RB, (d) (2.75×10^{-5} M) of AR, and (e) (2.70×10^{-3} M) curcumin (scale bar = 500 μm).

DOI: 10.1021/acsomega.8b02455
ACS Omega 2018, 3, 17751−17761

4.3. Surface Tension Measurement. Aggregation behavior of the ILBS is studied through measuring the surface tension of the aqueous ILBS solution at 25 ± 0.1 °C using K9 tensiometer (Kruss, Germany) with a platinum−iridium ring. The instrument was calibrated using triple-distilled water.

4.4. Dynamic Light Scattering and Zeta Potential Measurement. DLS and zeta potential were performed using Zetasizer, Nano-ZS, Malvern Instruments equipped with a built-in temperature controller having an accuracy of ±0.1 K. The measurements were made using a quartz cuvette having a path length of 1 cm. The data were analyzed using the standard algorithms and are reported with an uncertainty of less than 7%.

4.5. Turbidity Measurement. Turbidity of the solutions was measured on a Varian Carry 50 spectrophotometer (Varian, Switzerland). The instrument is equipped with a thermostatted cell compartment with a temperature accuracy of ±0.1 K. Samples were taken in the 1 cm path length quartz cuvette, and the absorbance was measured at 550 nm where no absorbance for both of the components was observed. All the measurements were performed in triplicate.

4.6. Optical Microscopy. A Nikon Eclipse TS 100 microscope was used to determine the size of coacervates. The microscope was equipped with a high intensity LED eco-illumination system.

4.7. Field Emission Scanning Electron Microscopy. A Hitachi S-4800 (Tokyo, Japan) field emission scanning electron microscope was used to measure the morphology of the complex coacervate formed through mixing C_8EMeImBr (112.5 mM) and NaSal (200 mM). The coacervate droplet was frozen on a clean silica wafer using liquid nitrogen. This will retain the microstructure of the coacervates. Then, the frozen sample was immediately lyophilized at −50 °C under vacuum. The lyophilized sample was then coated with a 1−2 nm thick Pt.

4.8. Construction of Phase Diagram. Stock solutions of C_8EMeImBr and NaSal were prepared separately. In the stoppered test tube with a cap, C_8EMeImBr was taken in a fixed amount and NaSal was added progressively under stirring so that the [C_8EMeImBr]/[NaSal] ratio varied. The mixtures were then vortexed and sonicated and allowed to equilibrate at a constant temperature in a water bath at 298 K. The phases were observed visually and their equilibrium state was assessed. The experiments were repeated to test for their reproducibility.

4.9. Sequestration of Dyes and Measurement of Partition Coefficients. Partition coefficients were measured by the ratio of the dye concentration present in the coacervate phase versus that in the dilute aqueous phase. Dyes and curcumin (stock solution) were added in the coacervate solution and the solution was vigorously vortexed for 10 min. Samples were left to stand for 24 h at 25 °C in the constant temperature bath, and both the coacervate and continuous aqueous phase were recovered separately in a sample tube. For curcumin, the mixture was diluted by a mixture of water and methanol (9:1 v/v). The samples were then analyzed for their absorbance by UV−visible spectroscopy at the λ_{max} for respective dyes for aqueous dilute phase. The intensity of a selected absorption peak was measured for the aqueous phase, and from that, the concentration of the dye/curcumin in the aqueous phase was determined. For the coacervate phase, the concentration of the dye/curcumin was determined through the relationship, $(C_0 - C_e)$, where C_0 is the initial concentration of dye, and C_e is the equilibrium concentration of dye in the aqueous dilute phase.

4.10. Epifluorescence Microscopy. The complex coacervate droplets formed by 112.5 mM of C_8EMeImBr and 200 mM of NaSal were visually inspected using a Zeiss "Axio Scope A1" model (Carl Zeiss Pvt Ltd, Oberkochen, Germany) and differential interference contrast filters. A drop (about 20 μL) of the premixed coacervate droplet solution mixed with the fluorescence dye (10 μL, 2.04×10^{-4} mM rhodamine 6G) was deposited on the glass slide surface, which was previously cleaned with dry ethanol. Fluorescence images were acquired using 40× magnification using an AxioCam MRc 5 camera under the control of AxioVision software.

■ ASSOCIATED CONTENT

Supporting Information

The Supporting Information is available free of charge on the ACS Publications website at DOI: 10.1021/acsomega.8b02455.

Table pertaining to sodium salicylate-induced micellar transition within various surfactant systems and visual images of coacervates before and after addition of 100 mm of $CaCl_2$, and sodium alginate (PDF)

■ AUTHOR INFORMATION

Corresponding Author

*E-mail: navedmalek@chem.svnit.ac.in, navedmalek@yahoo.co.in (N.I.M.).

ORCID

Omar A. El Seoud: 0000-0003-1683-5953

Naved I. Malek: 0000-0002-2164-5268

Notes

The authors declare no competing financial interest.

■ ACKNOWLEDGMENTS

M.K. acknowledges financial assistance of UGC-DAE for the Collaborative Research Scheme (UDCSR/MUM/AO/CRS-M-276/2017). The authors are thankful to Dr. Arvind Kumar (CSMCRI, Bhavnagar) and Dr. Ramesh L Gardas (IIT, Madras) for useful discussion. Authors are thankful to Dr. V.N. Lad (SVNIT, Surat) for the microscopy images and Dr. K. P. Patel (V.N.S.G. Univesity) for fluorescence imaging.

■ REFERENCES

(1) Myers, D. *Surfactant Science and Technology*; Wiley-Interscience, A John Wiley & Sons, Inc., Publication: Hoboken, New Jersey, 2006; pp 379−413.

(2) Bhattacharjee, J.; Aswal, V. K.; Hassan, P. A.; Pamu, R.; Narayanan, J.; Bellare, J. Structural evolution in catanionic mixtures of cetylpyridinium chloride and sodium deoxycholate. *Soft Matter* **2012**, *8*, 10130.

(3) Bungenberg de Jong, H. G.; Kruyt, H. R. *"Colloid Science"*; Elsevier Publishing Co.: Amsterdam, The Netherlands, 1959; Vol. 2, Chapter 8.

(4) Aumiller, W. M., Jr.; Pir Cakmak, F.; Davis, B. W.; Keating, C. D. RNA-Based Coacervates as a Model for Membraneless Organelles: Formation, Properties, and Interfacial Liposome Assembly. *Langmuir* **2016**, *32*, 10042−10053.

(5) Xu, Y.; Mazzawi, M.; Chen, K.; Sun, L.; Dubin, P. L. Protein Purification by Polyelectrolyte Coacervation: Influence of Protein Charge Anisotropy on Selectivity. *Biomacromolecules* **2011**, *12*, 1512−1522.

DOI: 10.1021/acsomega.8b02455
ACS Omega 2018, 3, 17751−17761

(6) Liu, W.; Zhao, W.-j.; Chen, J.-b.; Yang, M.-m. A cloud point extraction approach using Triton X-100 for the separation and preconcentration of Sudan dyes in chilli powder. *Anal. Chim. Acta* **2007**, *605*, 41−45.
(7) Appusamy, A.; John, I.; Ponnusamy, K.; Ramalingam, A. Removal of Crystal Violet Dye from Aqueous Solution Using Triton X-114 Surfactant via Cloud Point Extraction. *Eng. Sci. Technol. Int. J.* **2014**, *17*, 137−144.
(8) Zarei, A. R. Cloud point formation based on mixed micelle in the presence of electrolyte for extraction, preconcentration, and spectrophotometric determination of trace amounts of hydrazine in water and biological samples. *Anal. Biochem.* **2007**, *369*, 161−167.
(9) Sicilia, D.; Rubio, S.; Pérez-Bendito, D. Evaluation of the Factors Affecting Extraction of Organic Compounds Based on the Acid-Induced Phase Cloud Point Approach. *Anal. Chim. Acta* **2002**, *460*, 13−22.
(10) Wang, Z.; Larson, R. G. Molecular Dynamics Simulations of Threadlike Cetyltrimethylammonium Chloride Micelles: Effects of Sodium Chloride and Sodium Salicylate Salts. *J. Phys. Chem. B* **2009**, *113*, 13697−13710.
(11) Chiappisi, L.; Prévost, S.; Grillo, I.; Gradzielski, M. Chitosan/Alkylethoxy Carboxylates: A Surprising Variety of Structures. *Langmuir* **2014**, *30*, 1778−1787.
(12) Chiappisi, L.; Simon, M.; Gradzielski, M. Toward Bioderived Intelligent Nanocarriers for Controlled Pollutant Recovery and pH-Sensitive Binding. *ACS Appl. Mater. Interfaces* **2015**, *7*, 6139−6145.
(13) Wang, Y.; Banziger, J.; Dubin, P. L.; Filippelli, G.; Nuraje, N. Adsorptive Partitioning of an Organic Compound onto Polyelectrolyte-Immobilized Micelles on Porous Glass and Sand. *Environ. Sci. Technol.* **2001**, *35*, 2608−2611.
(14) Aumiller, W. M., Jr.; Keating, C. D. Phosphorylation-mediated RNA/peptide complex coacervation as a model for intracellular liquid organelles. *Nat. Chem.* **2015**, *8*, 129−137.
(15) Bidyut, K. P.; Satya, P. M.; Werner, K. *Ionic Liquid-Based Surfactant Science: Formulation, Characterization, and Applications*; John Wiley & Sons, Inc.: Hoboken, New Jersey, 2015; pp 63−99.
(16) More, U. U.; Vaid, Z. S.; Rajput, S. M.; Malek, N. I.; Seoud, O. A. Effects of 1-alkyl-3-methylimidazolium bromide ionic liquids on the micellar properties of [butanediyl-1,4-bis-(dimethyldodecylammonium bromide)] gemini surfactant in aqueous solution. *Colloid Polym. Sci.* **2017**, *295*, 2351−2361.
(17) Garcia, M. T.; Ribosa, I.; Perez, L.; Manresa, A.; Comelles, F. Aggregation Behavior and Antimicrobial Activity of Ester-Functionalized Imidazolium- and Pyridinium-Based Ionic Liquids in Aqueous Solution. *Langmuir* **2013**, *29*, 2536−2545.
(18) Liang, N.; Hou, X.; Huang, P.; Jiang, C.; Chen, L.; Zhao, L. Ionic liquid-based dispersive liquid-liquid microextraction combined with functionalized magnetic nanoparticle solid-phase extraction for determination of industrial dyes in water. *Sci. Rep.* **2017**, *7*, 13844.
(19) Vaid, Z. S.; Kumar, A.; El Seoud, O. A.; Malek, N. I. Drug Induced Micelle-to-Vesicle Transition in Aqueous Solutions of Cationic Surfactants. *RSC Adv.* **2017**, *7*, 3861−3869.
(20) Kuddushi, M.; Patel, N. K.; Rajput, S.; Shah, A.; El Seoud, O. A.; Malek, N. I. Thermo-Switchable de Novo Ionic Liquid-Based Gelators with Dye-Absorbing and Drug-Encapsulating Characteristics. *ACS Omega* **2018**, *3*, 12068−12078.
(21) Wang, X.; Yu, L.; Jiao, J.; Zhang, H.; Wang, R.; Chen, H. Aggregation Behavior of COOH-Functionalized Imidazolium-Based Surface Active Ionic Liquids in Aqueous Solution. *J. Mol. Liq.* **2012**, *173*, 103−107.
(22) Malek, N. I.; Vaid, Z. S.; More, U. U.; El Seoud, O. A. Ionic-Liquid-Based Surfactants with Unsaturated Head Group: Synthesis and Micellar Properties of 1-(n-Alkyl)-3-Vinylimidazolium Bromides. *Colloid Polym. Sci.* **2015**, *293*, 3213−3224.
(23) Morrissey, S.; Pegot, B.; Coleman, D.; Garcia, M. T.; Ferguson, D.; Quilty, B.; Gathergood, N. Biodegradable, non-bactericidal oxygen-functionalised imidazolium esters: A step towards 'greener' ionic liquids. *Green Chem.* **2009**, *11*, 475−483.
(24) Garcia, M. T.; Ribosa, I.; Perez, L.; Manresa, A.; Comelles, F. Aggregation Behavior and Antimicrobial Activity of Ester-Functionalized Imidazolium- and Pyridinium-Based Ionic Liquids in Aqueous Solution. *Langmuir* **2013**, *29*, 2536−2545.
(25) Goodchild, I.; Collier, L.; Millar, S. L.; Prokeš, I.; Lord, J. C. D.; Butts, C. P.; Bowers, J.; Webster, J. R. P.; Heenan, R. K. Structural studies of the phase, aggregation and surface behaviour of 1-alkyl-3-methylimidazolium halide + water mixtures. *J. Colloid Interface Sci.* **2007**, *307*, 455−468.
(26) Rajput, S. M.; Kumar, S.; Aswal, V. K.; El Seoud, O. A.; Malek, N. I.; Kailasa, S. K. Drug-Induced Micelle-to-Vesicle Transition of a Cationic Gemini Surfactant: Potential Applications in Drug Delivery. *ChemPhysChem* **2018**, *19*, 865−872.
(27) Moulik, S. P.; Haque, M. E.; Jana, P. K.; Das, A. R. Micellar Properties of Cationic Surfactants in Pure and Mixed States. *J. Phys. Chem.* **1996**, *100*, 701−708.
(28) Dong, B.; Li, N.; Zheng, L.; Yu, L.; Inoue, T. Surface adsorption and micelle formation of surface active ionic liquids in aqueous solution. *Langmuir* **2007**, *23*, 4178−4182.
(29) Wang, X.; Yu, L.; Jiao, J.; Zhang, H.; Wang, R.; Chen, H. Aggregation behavior of COOH-functionalized imidazolium-based surface active ionic liquids in aqueous solution. *J. Mol. Liq.* **2012**, *173*, 103−107.
(30) Dong, B.; Zhao, X.; Zheng, L.; Zhang, J.; Li, N.; Inoue, T. Aggregation behavior of long-chain imidazolium ionic liquids in aqueous solution: Micellization and characterization of micelle microenvironment. *Colloids Surf., A* **2008**, *317*, 666−672.
(31) Israelachvili, J. N.; Mitchell, D. J.; Ninham, B. W. Theory of self-assembly of hydrocarbon amphiphiles into micelles and bilayers. *J. Chem. Soc., Faraday Trans. 2* **1976**, *72*, 1525−1568.
(32) Evans, D. F.; Wennerström, F. Where Physics, Chemistry, Biology, and Technology. *The Colloidal Domain*, 2nd ed.; Wiley-VCH, 1999; p 632.
(33) Cornellas, A.; Perez, L.; Comelles, F.; Ribosa, I.; Manresa, A.; Garcia, M. T. Self-aggregation and antimicrobial activity of imidazolium and pyridinium based ionic liquids in aqueous solution. *J. Colloid Interface Sci.* **2011**, *355*, 164−171.
(34) Gómez-Díaz, D.; Navaza, J. M.; Sanjurjo, B. Density, Kinematic Viscosity, Speed of Sound, and Surface Tension of Hexyl, Octyl, and Decyl Trimethyl Ammonium Bromide Aqueous Solutions. *J. Chem. Eng. Data* **2007**, *52*, 889−891.
(35) Vaid, Z. S.; Rajput, S. M.; Shah, A.; Kadam, Y.; Kumar, A.; El Seoud, O. A.; Mata, J. P.; Malek, N. I. Salt-Induced Microstructural Transitions in Aqueous Dispersions of Ionic-Liquids-Based Surfactants. *ChemistrySelect* **2018**, *3*, 4851−4858.
(36) Dai, C.; Wu, X.; Li, W.; You, Q.; Zhao, M.; Du, M.; Liu, Y.; Li, Y. The role of hydroxyethyl groups in the construction of wormlike micelles in the system of quaternary ammonium surfactant and sodium salicylate. *Soft Matter* **2015**, *11*, 7817−7826.
(37) Douliez, J.-P.; Martin, N.; Gaillard, C.; Beneyton, T.; Baret, J.-C.; Mann, S.; Beven, L. Catanionic Coacervate Droplets as a Surfactant-Based Membrane-Free Protocell Model. *Angew. Chem., Int. Ed.* **2017**, *56*, 13689−13693.
(38) Anderson, D.; Wennerstroem, H.; Olsson, U. Isotropic bicontinuous solutions in surfactant-solvent systems: The L3 phase. *J. Phys. Chem.* **1989**, *93*, 4243−4253.
(39) Menger, F. M.; Peresypkin, A. V.; Caran, K. L.; Apkarian, R. P. A Sponge Morphology in an Elementary Coacervate. *Langmuir* **2000**, *16*, 9113−9116.
(40) Banjare, M. K.; Kurrey, R.; Yadav, T.; Sinha, S.; Satnami, M. L.; Ghosh, K. K. A comparative study on the effect of imidazolium-based ionic liquid on self-aggregation of cationic, anionic and nonionic surfactants studied by surface tension, conductivity, fluorescence and FTIR spectroscopy. *J. Mol. Liq.* **2017**, *241*, 622−632.
(41) Antonov, M.; Mazzawi, M.; Dubin, P. L. Entering and Exiting the Protein−Polyelectrolyte Coacervate Phase via Nonmonotonic Salt Dependence of Critical Conditions. *Biomacromolecules* **2010**, *11*, 51−59.

DOI: 10.1021/acsomega.8b02455
ACS Omega 2018, 3, 17751−17761

(42) Sarah, M. The Impact of Salts on Single Chain Amphiphile Membranes and Implications for the Location of the Origin of Life. *Life* **2017**, *7*, 44.
(43) Perry, S.; Li, Y.; Priftis, D.; Leon, L.; Tirrell, M. The Effect of Salt on the Complex Coacervation of Vinyl Polyelectrolytes. *Polymers* **2014**, *6*, 1756−1772.
(44) Monnard, P.-A.; Apel, C. L.; Kanavarioti, A.; Deamer, D. W. Influence of Ionic Inorganic Solutes on Self-Assembly and Polymerization Processes Related to Early Forms of Life: Implications for a Prebiotic Aqueous Medium. *Astrobiology* **2002**, *2*, 139−152.
(45) Wu, T.; Oake, J.; Liu, Z.; Bohne, C.; Branda, N. R. Probing the Microenvironments in a Polymer-Wrapped Core-Shell Nanoassembly Using Pyrene Chromophores. *ACS Omega* **2018**, *3*, 7673−7680.
(46) Vaid, Z. S.; Rajput, S. M.; Kuddushi, M.; Kumar, A.; El Seoud, O. A.; Malek, N. I. Synergistic Interaction between Cholesterol and Functionalized Ionic Liquid Based Surfactant Leading to the Morphological Transition. *ChemistrySelect* **2018**, *3*, 1300−1308.
(47) Lazaridis, N. K.; Kyzas, G. Z.; Vassiliou, A. A.; Bikiaris, D. N. Chitosan Derivatives as Biosorbents for Basic Dyes. *Langmuir* **2007**, *23*, 7634−7643.
(48) Knaapila, M.; Costa, T.; Garamus, V. M.; Kraft, M.; Drechsler, M.; Scherf, U.; Burrows, H. D. Polyelectrolyte Complexes of a Cationic All Conjugated Fluorene-Thiophene Diblock Copolymer with Aqueous DNA. *J. Phys. Chem. B* **2015**, *119*, 3231−3241.
(49) Zhao, W.; Fan, Y.; Wang, H.; Wang, Y. Coacervate of Polyacrylamide and Cationic Gemini Surfactant for the Extraction of Methyl Orange from Aqueous Solution. *Langmuir* **2017**, *33*, 6846−6856.
(50) Karahaliloğlu, Z. Curcumin-loaded silk fibroin e-gel scaffolds for wound healing applications. *Mater. Technol.* **2018**, *33*, 276−287.

DOI: 10.1021/acsomega.8b02455
ACS Omega 2018, 3, 17751−17761